

The $\pi^+\pi^-$ Coulomb interaction study and its use in the data processing

B.Adeva,¹ L.Afanasyev,² A.Anania,³ S.Aogaki,⁴ A.Benelli,⁵ V.Brekhovskikh,⁶ T.Cechak,⁵ M.Chiba,⁷ P.Chliapnikov,⁶ D.Drijard,^{5,8} A.Dudarev,² D.Dumitriu,⁴ P.Federicova,⁵ A.Gorin,⁶ K.Gritsay,² C.Guaraldo,⁹ M.Gugiu,⁴ M.Hansroul,⁸ Z.Hons,¹⁰ S.Horikawa,¹¹ Y.Iwashita,¹² J.Kluson,⁵ M.Kobayashi,¹³ L.Kruglova,² A.Kulikov,² E.Kulich,² A.Lamberto,³ A.Lanaro,¹⁴ R.Lednický,¹⁵ C.Mariñas,¹ J.Martincik,⁵ L.Nemenov,^{2,*} M.Nikitin,² K.Okada,¹⁶ V.Olchevskii,² M.Pentia,⁴ A.Penzo,¹⁷ M.Plo,¹ P.Prusa,⁵ G.Rappazzo,³ A.Romero Vidal,¹ A.Ryazantsev,⁶ V.Rykalin,⁶ J.Saborido,¹ J.Schacher,¹⁸ A.Sidorov,⁶ J.Smolik,⁵ F.Takeutchi,¹⁶ T.Trojek,⁵ S.Trusov,¹⁹ T.Urban,⁵ T.Vrba,⁵ V.Yazkov,^{19,†} Y.Yoshimura,¹³ and P.Zrelov²

(DIRAC Collaboration)

¹*Santiago de Compostela University, Spain*

²*JINR Dubna, Russia*

³*Messina University, Messina, Italy*

⁴*IFIN-HH, National Institute for Physics and Nuclear Engineering, Bucharest, Romania*

⁵*Czech Technical University in Prague, Czech Republic*

⁶*IHEP Protvino, Russia*

⁷*Tokyo Metropolitan University, Japan*

⁸*CERN, Geneva, Switzerland*

⁹*INFN, Laboratori Nazionali di Frascati, Frascati, Italy*

¹⁰*Nuclear Physics Institute ASCR, Rez, Czech Republic*

¹¹*Zurich University, Switzerland*

¹²*Kyoto University, Kyoto, Japan*

¹³*KEK, Tsukuba, Japan*

¹⁴*University of Wisconsin, Madison, USA*

¹⁵*Institute of Physics ASCR, Prague, Czech Republic*

¹⁶*Kyoto Sangyo University, Kyoto, Japan*

¹⁷*INFN, Sezione di Trieste, Trieste, Italy*

¹⁸*Albert Einstein Center for Fundamental Physics,*

Laboratory of High Energy Physics, Bern, Switzerland

¹⁹*Skobeltsyn Institute for Nuclear Physics of Moscow State University, Moscow, Russia*

(Dated: September 20, 2024)

In this work the Coulomb effects (Coulomb correlations) in $\pi^+\pi^-$ pairs produced in $p + \text{Ni}$ collisions at 24 GeV/c, are studied using experimental $\pi^+\pi^-$ pair distributions in Q , the relative momentum in the pair center of mass system (c.m.s), and its projections Q_L (longitudinal component) and Q_t (transverse component) relative to the pair direction in the laboratory system (l.s.). The major part of the pion pairs (*Coulomb pairs*) is produced in the decay of ρ, ω and Δ -resonances and other short-lived sources. In these pairs, the significant Coulomb interaction occurs at small Q , dominating the $\pi^+\pi^-$ interaction in the final state.

The minor part of the pairs (*non-Coulomb pairs*) is produced if one or both pions arose from long-lived sources like η, η' or from different interactions. In this case, the final state interaction is practically absent.

The Q, Q_L , and Q_t distributions of the *Coulomb pairs* in the c.m.s. have been simulated assuming they are described by the phase space modified by the known point-like Coulomb correlation function $A_C(Q)$, corrected for small effects due to the nonpoint-like pair production and the strong two-pion interaction. The same distributions of *non-Coulomb pairs* have been simulated according to the phase space, but without $A_C(Q)$.

In all Q_t intervals, the experimental Q_L spectrum shows a peak around $Q_L = 0$ caused by the Coulomb final state interaction. The full width at half maximum increases with Q_t from 3 MeV/c for $0 < Q_t < 0.25$ MeV/c to 11 MeV/c for $4.0 < Q_t < 5.0$ MeV/c. The experimental Q_L distributions have been fitted with two free parameters: the fraction of *Coulomb pairs* and the normalization constant. The precision of the description of these distributions is better than 2% in Q_t intervals 2–3, 3–4, and 4–5 MeV/c, and better than 0.5% in the total Q_t interval 0–5 MeV/c.

It is shown that the number of *Coulomb pairs* in all Q_t intervals, including the small Q_t (small opening angles θ in the l.s.) is calculated with the theoretical precision better than 2%.

The comparison of the simulated and experimental numbers of *Coulomb pairs* at small Q_t allows us to check and correct the detection efficiency for the pairs with small θ (0.06 mrad and smaller).

It is shown that *Coulomb pairs* can be used as a new physical tool to check and correct the quality of the simulated events. The special property of the *Coulomb pairs* is the possibility of checking and correcting the detection efficiency, especially for the pairs with small opening angles.

* Corresponding author; nemenov@cern.ch

† deceased

I. INTRODUCTION

The Coulomb interaction effect was first observed and investigated in the hadron pair production in [1]. The pairs were produced in the reaction

$$p + \text{Ta} \longrightarrow \pi^+\pi^- + X \quad (1)$$

at the proton momentum of 70 GeV/c. The generation of the pairs (*Coulomb pairs*) was described [2] as the product of the pair production matrix element without Coulomb interaction in the final state and the Coulomb correlation function $A_C(Q)$ [3–6], where Q is the relative momentum in the pair center of mass system (c.m.s). This approach was used by analogy with the theoretical description of the Coulomb final state interaction in e^+e^- pair production in photon-nucleus interaction [6]. In both cases the pair production region $\sim 1/m$ (m is the pion or electron mass) is two orders of magnitude smaller than the distance $R \sim 1/\alpha m$ ($\alpha = 1/137$ is the fine structure constant) over which the wave function of the relative motion of the particles changes. It allows one to use the wave function value at $r = 0$.

The Q distribution [1] of $\pi^+\pi^-$ pairs produced in one p+Ta interaction (*prompt pairs*) $F(Q)_{pr}$ was divided by the same distribution $F(Q)_{acc}$ of the *accidental pairs* generated at two different production points, without interaction in the final state. This ratio $R(Q)_{exp} = F(Q)_{pr}/F(Q)_{acc}$ is normalized to unity at the large Q and describes, by definition, the $\pi^+\pi^-$ final state interaction dependence on Q (Coulomb correlation function).

The theoretical ratio $R(Q)_{calc}$ was evaluated with the phase space restrictions due to setup acceptance and Coulomb interaction in the final state. It was shown that $R(Q)_{calc}$ described well the ratio $R(Q)_{exp}$ in the total analyzed Q interval 0 – 40 MeV/c. The Coulomb correlation function increases when Q decreases. In (1) the $R(Q)_{exp}$ value increased 6 times when Q decreased from 40 MeV/c to 0.5 MeV/c. The function R_{exp} dependence on Q_L (longitudinal component) and Q_t (transverse component) was also well described.

The Q_L distribution of the prompt $\pi^+\pi^-$ pairs was analyzed using the following procedure. For an experimental accidental pion pair with Q_L , the weight $A_C(Q_L)$ was introduced to "create" a *Coulomb pair*. *Coulomb pairs* are generated when π^+ and π^- are produced from the decay of ρ, ω, Δ and other short-lived sources. If one or both pions are produced from long-lived sources like η, η' or K^0 's, then the distance between particles is larger and the Coulomb interaction in the final state is almost absent. These pairs were defined as "non-Coulomb" pairs ("decay pairs" in [1]) and their distribution in Q_L was the same as the Q_L spectrum of the accidental pairs. The experimental Q_L distribution was described by the sum of the *Coulomb* and *non-Coulomb* pairs. The ratio between the *Coulomb* and *non-Coulomb* pairs was taken from the Lund model [7]. The experimental Q_L spectrum was well

fitted with one free parameter - the normalization constant.

The Coulomb effects in the $\pi^+\pi^-$ and $p\pi^-$ pairs were observed and described in [8].

The pairs with the Coulomb interaction in the final state create the main background for the observation and investigation of the $\pi^+\pi^-$ atoms [2]. Therefore, to observe $\pi^+\pi^-$ atoms, the *Coulomb pair* distributions must be described accurately. A detailed description of the $\pi^+\pi^-$ pair spectrum was given in [9], where $\pi^+\pi^-$ atoms were observed for the first time. The $\pi^+\pi^-$ pairs in proton-nucleus interaction are produced on any target in the processes shown in Fig.1 (Ni target).

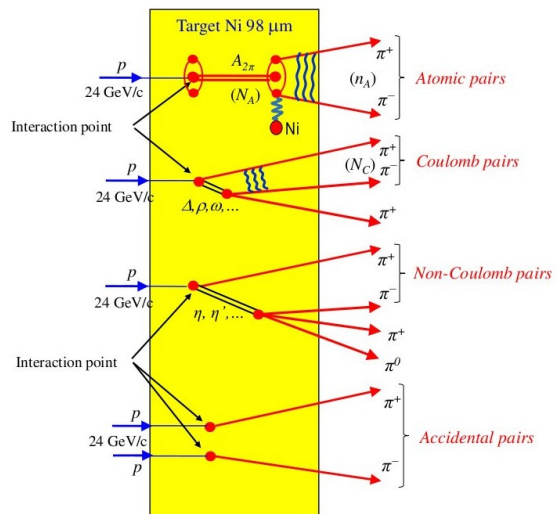


FIG. 1. The atomic, Coulomb, non-Coulomb, and accidental pair production processes. The wave lines denote the Coulomb interaction.

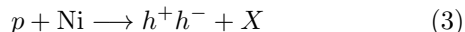
The $\pi^+\pi^-$ atoms produced in the p+Ta interaction are broken up (ionized) with a large probability while moving in the target, which results in generation of $\pi^+\pi^-$ pairs (*atomic pairs*). Since *non-Coulomb* and *accidental pairs* are uncorrelated and indistinguishable in the momentum space, we call here their sum *non-Coulomb pairs*. The relative momentum Q of *atomic pairs* is less than 3 MeV/c for thin targets ($10^{-3}X_0$). Due to this specific kinematical feature, *atomic pairs* are experimentally observable. These pairs number n_A we need to measure the $\pi^+\pi^-$ atom lifetime and the $\pi^+\pi^-$ scattering length in the s -state. To evaluate the n_A number, the *Coulomb* and *non-Coulomb* pairs (Q, Q_L) distributions are described in a wide interval of these parameters. Then the fitting distributions are subtracted from the total (Q, Q_L) spectrum. The precision of the *Coulomb pair* spectrum defines the accuracy of n_A and the error of the $\pi^+\pi^-$ scattering length.

The distributions in Q_L and the Q_t components Q_x and Q_y are Gaussian-like and have different standard deviations (s.d.) σ_L, σ_X and σ_Y . Therefore, the prompt $\pi^+\pi^-$ distribution was analyzed using the parameter

$$F = \sqrt{\left(\frac{Q_L}{\sigma_L}\right)^2 + \left(\frac{Q_X}{\sigma_X}\right)^2 + \left(\frac{Q_Y}{\sigma_Y}\right)^2} \quad (2)$$

The *Coulomb* and *non-Coulomb pair* distributions as the function of F were obtained in the same way as the pair distributions in Q_L described above. It was shown that the prompt pair spectrum in F in the interval 0–40 MeV/ c is well described as the sum of the *Coulomb* and *non-Coulomb pairs* distribution with two free parameters: the normalization constant and the ratio *Coulomb* to *non-Coulomb pairs*.

A more precise description of the *Coulomb* and *non-Coulomb pairs* was done in the DIRAC experiment [10] at CERN in the measurement of the $\pi^+\pi^-$ atom lifetime and the $\pi\pi$ scattering length. In this experiment $\pi^+\pi^-$, π^+K^- , π^-K^+ , K^+K^- and $p\bar{p}$ hadron pairs were generated in the process



with the proton momentum of 24 GeV/ c .

The Q distribution of *Coulomb pair* was simulated assuming they are described by the phase space modified by the Coulomb correlation function $A_C(Q)$. The same spectrum of the *non-Coulomb pairs* was simulated (without $A_C(Q)$). The c.m.s. pion momenta were transformed to the l.s. using the experimental total momentum of the $\pi^+\pi^-$ pairs. The difference between the total momentum distribution of the *Coulomb* and *non-Coulomb pairs* was taken into account using FRITIOF-6 code [11]. This approach allowed a good description of the Q and Q_L distributions. In the second DIRAC experiment [12] larger experimental data were analyzed.

Coulomb pair simulation in [12] included the Coulomb and strong $\pi^+\pi^-$ interactions in the final state and the influence of the nonpoint-like pair production on the spectrum shape [13]. The sources of the nonpoint-like *Coulomb pair* production were investigated in [14]. A new procedure [15, 16] was used, which more accurately took into account the difference between the total momentum distributions of the *Coulomb* and *non-Coulomb pairs* in the l.s. This analysis enabled a good description of the *Coulomb pair* distribution in Q_L and Q_t in the intervals 0–15 MeV/ c and 0–5 MeV/ c respectively.

The DIRAC setup was upgraded to identify and investigate $\pi^+\pi^-$, π^+K^- , π^-K^+ , K^+K^- and $p\bar{p}$ pairs [17]. In the dedicated experiment [18], distributions of *Coulomb*, *non-Coulomb* and *atomic* π^+K^- and π^-K^+ pairs were accurately described. An improved version of the simulation procedure and a more accurate setup geometry tuning were used [19].

This allowed us to observe for the first time the π^+K^- and π^-K^+ atoms, to measure their lifetime and to evaluate the πK scattering length. In all those investigations the $\pi^+\pi^-$ pairs as the background processes were used to check the setup tuning [19]. The same simulation procedure was used in the present work.

The Coulomb interaction in the final state was studied both theoretically and experimentally in [1–6, 8–10, 12–18] before our reported investigations. In this Introduction, we present the theoretical description of the Coulomb interaction and its use in analyzing the experimental results in the works cited above.

The present work (see also [20]) deals with the principal new investigation of the $\pi^+\pi^-$ pairs detected by the upgraded DIRAC setup [17] with new detectors for suppression of K mesons, protons, and antiprotons. It allowed one to decrease the admixture of K^+K^- and $p\bar{p}$ pairs in the pion pair data. It was shown that selection of two-pion *Coulomb pairs* in sufficiently narrow Q_t intervals makes it possible to control the width of the Coulomb peak of the Q_L distribution around $Q_L = 0$ and describe it with a precision better than 2%. This enables using the *Coulomb pairs* as a new physical tool to check and correct the detector resolution and efficiency, especially for the pairs with opening angle θ in the l.s. down to about 0.02 mrad.

II. SETUP AND EXPERIMENTAL CONDITIONS

The aim of the magnetic two-arm vacuum spectrometer [17, 21–23] (Fig. 2) is to detect and identify K^+K^- , $\pi^+\pi^-$, π^-K^+ , and π^+K^- pairs with small Q . The structure of K^+K^- and $\pi^+\pi^-$ pairs downstream the magnet is approximately symmetric. The 24 GeV/ c primary proton beam, extracted from the CERN PS, hit a Ni target of the $(108 \pm 1)\mu\text{m}$ thickness or $7.4 \cdot 10^{-3}X_0$.

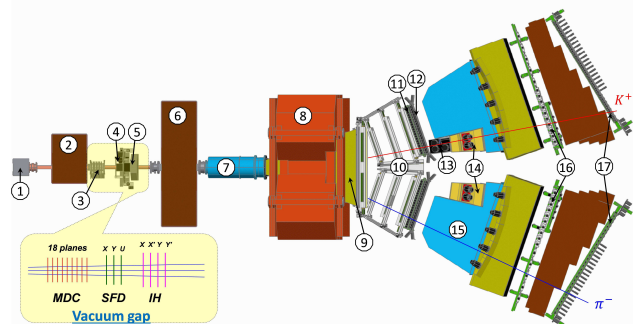


FIG. 2. General view of the DIRAC setup (1 – target station; 2 – first shielding; 3 – micro drift chambers (MDC); 4 – scintillating fiber detector (SFD); 5 – ionization hodoscope (IH); 6 – second shielding; 7 – vacuum tube; 8 – spectrometer magnet; 9 – vacuum chamber; 10 – drift chambers (DC); 11 – vertical hodoscope (VH); 12 – horizontal hodoscope (HH); 13 – aerogel Cherenkov (ChA); 14 – heavy gas Cherenkov (ChF); 15 – nitrogen Cherenkov (ChN); 16 – preshower (PSh); 17 – muon detector (Mu).

The axis of the secondary channel is inclined relative to the proton beam by 5.7° upward. The solid angle of the

channel is $\Omega = 1.2 \cdot 10^{-3}$ sr. Secondary particles propagate mainly in vacuum to the Al foil ($7.6 \cdot 10^{-3} X_0$) at the exit of the vacuum chamber, which is installed between the poles of the dipole magnet ($B_{max} = 1.65$ T and $BL = 2.2$ Tm). In the vacuum channel gap, 18 planes of the Micro Drift Chambers (MDC) and (X , Y , U) planes of the Scintillation Fiber Detector (SFD) were installed to measure both the particle coordinates ($\sigma_{SFDx} = \sigma_{SFDy} = 60$ μm , $\sigma_{SFDu} = 120$ μm) and the particle time ($\sigma_{tSFDx} = 380$ ps, $\sigma_{tSFDy} = \sigma_{tSFDu} = 520$ ps). The total matter radiation thickness between the target and the vacuum chamber amounts to $7.7 \cdot 10^{-2} X_0$.

Each spectrometer arm is equipped with the following subdetectors [17]: drift chambers (DC) to measure particle coordinates with approximately 85 μm precision and to evaluate the particle path length; a vertical hodoscope (VH) to determine particle times with 110 ps accuracy for identification of equal mass pairs via the time of flight (TOF) between the SFDx plane and the VH; a horizontal hodoscope (HH) to select particles with a vertical distance less than 75 mm (Q_Y less than 15 MeV/c) in the two arms; an aerogel Cherenkov counter (ChA) to distinguish kaons from protons; a heavy gas (C_4F_{10}) Cherenkov counter (ChF) to distinguish pions from kaons and protons; a nitrogen Cherenkov (ChN) and preshower (PSh) detectors to identify and reject e^+e^- pairs; an iron absorber and a two-layer scintillation counter (Mu) to identify muons. In the negative arm, no aerogel Cherenkov counter was installed, because the number of antiprotons is small compared to K^- .

Pairs of oppositely charged particles, produced in one p+Ni interaction (prompt pairs) and accidentals produced in two different interactions in the time interval ± 20 ns are selected by requiring a 2-arm coincidence (ChN in anticoincidence) with the coplanarity restriction (HH) in the first-level trigger. The second-level trigger selects events with at least one track in each arm by exploiting the DC-wire information (track finder). Particle pairs π^-p ($\pi^+\bar{p}$) from Λ ($\bar{\Lambda}$) decay were used for spectrometer calibration, and e^+e^- pairs were employed for general detector calibration.

III. DATA PROCESSING

The collected events were analyzed with the DIRAC reconstruction program ARIANE [24].

A. Tracking

Only events with one or two particle tracks in the DC of each arm are processed. The event reconstruction is performed as follows [18]:

- One or two hadron tracks are identified in the DC of each arm with hits in VH, HH, and PSh slabs and no signal in ChN and Mu.

- Track segments reconstructed in the DC are extrapolated backward to the beam position in the target, using the transfer function of the dipole magnet and the program ARIANE. This procedure provides approximate particle momenta and the corresponding points of intersection in the MDC, SFD, and IH.
- Hits are searched for around the expected SFD coordinates in the region ± 1 cm corresponding to (3–5) σ_{pos} defined by the position accuracy with allowance for the particle momenta. To identify the event when two particles cross the same SFD column, the double ionization in the corresponding IH slab was requested.

The momentum of the positively or negatively charged particle is refined to match the X -coordinates of the DC tracks as well as the SFD hits in the X - or U -plane, depending on the presence of hits. To find the best 2-track combination, the two tracks should not use a common SFD hit in the case of more than one hit in the proper region. In the final analysis, the combination with the best χ^2 in the other SFD planes is kept.

B. Setup tuning with Λ and $\bar{\Lambda}$ particles

To check the general geometry of the DIRAC experiment, Λ and $\bar{\Lambda}$ particles decaying into $p\pi^-$ and $\pi^+\bar{p}$ in our setup were used [19]. After the setup tuning the weighted average of the experimental Λ mass overall runs, $M_{\Lambda}^{\text{DIRAC}} = (1.115680 \pm 2.9 \cdot 10^{-6})$ GeV/ c^2 , agrees very well with the PDG value, $M_{\Lambda}^{\text{PDG}} = (1.115683 \pm 6 \cdot 10^{-6})$ GeV/ c^2 . The weighted average of the experimental $\bar{\Lambda}$ mass is $M_{\bar{\Lambda}}^{\text{DIRAC}} = (1.11566 \pm 1 \cdot 10^{-5})$ GeV/ c^2 . This demonstrates that the geometry of the DIRAC setup is well described.

The width of the Λ mass distribution allows testing the momentum and angular resolution of the setup in the simulation. The processed events were collected in the Data 1, Data 2, and Data 3 samples, during three different runs. Table I shows a good agreement between the simulated and experimental Λ widths in Data 2 and Data 3. A further test consists of comparing the experimental Λ and $\bar{\Lambda}$ widths.

TABLE I. The Λ width in GeV/ c^2 for the experimental and MC data and the $\bar{\Lambda}$ width for the experimental data.

	Λ width (data) GeV/ c^2	Λ width (MC) GeV/ c^2	$\bar{\Lambda}$ width (data) GeV/ c^2
Data 2	$4.42 \cdot 10^{-4} \pm 7.4 \cdot 10^{-6}$	$4.42 \cdot 10^{-4} \pm 4.4 \cdot 10^{-6}$	$4.5 \cdot 10^{-4} \pm 3 \cdot 10^{-5}$
Data 3	$4.41 \cdot 10^{-4} \pm 7.5 \cdot 10^{-6}$	$4.37 \cdot 10^{-4} \pm 4.5 \cdot 10^{-6}$	$4.3 \cdot 10^{-4} \pm 2 \cdot 10^{-5}$

The average value of the correction that was introduced in the simulated width is $1.00203 \pm 0.00191 \cdot 10^{-3}$. Therefore, nonsignificant corrections were introduced in the l.s. particle momenta.

C. Event selection

Equal-mass pairs contained in the selected event sample are classified into three categories: $\pi^+\pi^-$, K^+K^- , and $p\bar{p}$ pairs.

The classification is based on the TOF measurement [25] for the distance between the SFD X-plane and the VH of about 11m. For pairs with a total momenta range from 3.8 to 8 GeV/c, additional information from the Heavy Gas Cherenkov (ChF) counters (Section II) is used to better separate $\pi^+\pi^-$ from K^+K^- and $p\bar{p}$ pairs. The ChF counters detect pions in this region with (95–97)% efficiency [26], whereas kaons and protons (antiprotons) do not generate any signal.

IV. DESCRIPTION OF $\pi^+\pi^-$ PAIR PRODUCTION AND THE SIMULATION PROCEDURE

The experimental distributions of the Coulomb and non-Coulomb pairs in the relative momentum Q and its components were compared with the corresponding simulated distributions.

The simulated Coulomb $\pi^+\pi^-$ spectra in the pair c.m.s. were calculated using the relation

$$\frac{dN}{dQ_i} = |M_{\text{prod}}|^2 F(Q_i) A_C(Q_i) D(Q_i) \quad (4)$$

where Q_i is Q , Q_L or Q_t , M_{prod} is the production matrix element without Q dependence in the investigated Q interval, $F(Q_i)$ is the phase space and $A_C(Q)$ is the Coulomb correlation function

$$A_C(Q) = \frac{2\pi m_\pi \alpha / Q}{1 - \exp(-2\pi m_\pi \alpha / Q)} \quad (5)$$

with allowance for the Coulomb final state interaction (FSI).

For small and large Q the respective Coulomb correlation function values are

$$A_C = 2\pi m_\pi \alpha / Q \quad \text{and} \quad A_C = 1 \quad (6)$$

The function $A_C(Q)$ in formula (5) describes the Coulomb final state interaction of nonrelativistic particles. The function describing the same interaction of relativistic particles was evaluated in [27].

The function $D(Q_i)$ in Eq. (4) takes into account small corrections caused by strong two-pion interaction in the final state and nonpoint-like pair production [13]. The D -function dependence on Q was calculated in [13] using the space-time distribution of the pion production points based on the UrQMD transport code simulation [28], taking into account particle re-scatterings and resonance decays, including short-lived, intermediate (ω), and long-lived (η') resonances. Within possible uncertainties of the ω and η' fractions, it was shown that in the analyzed Q interval up to 20 MeV/c, the correction D function could

be approximated as $D(Q) = c + bQ$ with $c = 1.01 - 1.06$ and $|b| < 0.5/\text{GeV}/c$. The slope parameter b strongly depends on the ω and η' fractions, changing from $-0.5/\text{GeV}$ when they are ignored to $+0.5/\text{GeV}$ when they are taken into account. Detailed analysis and evaluation of various resonance contributions to the production of the $\pi^+\pi^-$ at small Q was done in [14]. Since the estimated variation of the correction function $D(Q)$ in the interval 0–20 MeV/c is less than 1%, one may describe the Q distribution of the $\pi^+\pi^-$ Coulomb pairs with this precision taking into account only the point-like Coulomb interaction. One can further improve this precision by taking into account the strong two-pion interaction and finite space-time separation of pion production points. In the present work, the correction function $D(Q)$ from [13] was used to describe the Q_L and Q_t distributions.

The same simulation was done for the non-Coulomb $\pi^+\pi^-$ pairs using formula (4) without the correlation function $A_C(Q)$. The Q_L distributions of non-Coulomb and accidental pairs are the same. Therefore, in all analyses presented below the numbers of non-Coulomb pairs include the contribution of accidental pairs.

To calculate the momenta of the pair particles in the laboratory system (l.s.), the l.s. pair momentum is added to the c.m.s. one considering the difference between the total momentum distributions of the Coulomb and non-Coulomb pairs in the l.s. [15, 16]. This allows calculating the momenta \vec{P}^+ and \vec{P}^- of the π^+ and π^- in the l.s. and their total momentum $\vec{P} = \vec{P}^+ + \vec{P}^-$. By using the dedicated GEANT-DIRAC code, the simulated pairs are propagated through the setup with allowance for the multiple scattering and the response of the detectors in front of the magnet - the Scintillator Fiber Detector (SFD) and the Ionization Detector (ID).

The distance D between two particles in the l.s. decreases with Q_t and for small D in this experiment, the coordinate scintillation fiber detector with some probability cannot distinguish a one-particle hit from a two-particle hit. In this case, the amplitude is measured in the ionization detector. If the amplitude is higher than some threshold, this event is considered a two-particle hit. The introduction of the threshold results in rejecting part of the pairs and decreasing their detection efficiency ϵ . This decrease begins with D reducing below 0.8 mm in the x and y projections; the corresponding pair opening angle projections are 0.28 mrad. Behind the spectrometer magnet, only events with one or two tracks per arm are selected.

On the basis of the information from the detectors, the events were reconstructed by the ARIANE code and processed as experimental pairs. The simulated event distribution in \vec{P}_{lab} was tuned by requiring that the Coulomb and non-Coulomb pairs fit the experimental $\pi^+\pi^-$ pair spectrum in $\vec{P}_{\text{exp}} = \vec{P}_{\text{exp}}^+ + \vec{P}_{\text{exp}}^-$ where \vec{P}_{exp}^+ and \vec{P}_{exp}^- are the experimental l.s. momenta of π^+ and π^- . After this the Q_L , Q_t and Q distributions of the simulated events were calculated and compared with the experimental spectra.

V. ANALYSIS OF EXPERIMENTAL Q_L DISTRIBUTIONS OF $\pi^+\pi^-$ PAIRS AND MEASUREMENT OF THE NUMBER OF COULOMB AND NON-COULOMB PAIRS

For the analysis [20], events with the time difference between the VH arms less than 0.5 ns were selected. These pair distributions in Q_L were separately fitted in three data samples by a combination of the simulated *Coulomb* and *non-Coulomb pair* distributions in nine Q_t intervals: 0–0.25 (1), 0.25–0.5, 0.5–0.75, 0.75–1, 0–1 (2), 1–2, 2–3 (3), 3–4 and 4–5 MeV/c (4). Four of them are marked by numbers in parentheses for further reference.

The ratio between these pair numbers in each interval was a free parameter. The fitting interval $-20 \text{ MeV}/c < Q_L < 20 \text{ MeV}/c$ did not include the region $-2 \text{ MeV}/c < Q_L < 2 \text{ MeV}/c$ which involves atomic pairs having different shapes of the Q_L and Q_t spectra. The number of simulated events for each data sample is an order of magnitude larger than the number of the corresponding experimental events.

Figure 3 shows the sum of three samples of experimental and fitting distributions in intervals (1) – (4). Also, the fitting distributions of the *Coulomb* and *non-Coulomb pairs* are presented separately. The excess events in the interval $-2 \text{ MeV}/c < Q_L < 2 \text{ MeV}/c$ are due to the atomic pairs. The experimental *Coulomb pair* spectrum shows the peak around $Q_L = 0$. The full width at half maximum increases with Q_t , and for Q_t intervals 1, 2, 3, and 4 the width values are 3.4 MeV/c, 4 MeV/c, 6.5 MeV/c and 11 MeV/c respectively. They were obtained by measuring the histogram parameters.

The *Coulomb pair* distributions in Q_L for Q_t intervals (1) – (4) at the pair production point were evaluated using formula (4) and are presented in Fig. 4.

The full width at half maximum for the four Q_t intervals is 1.0 MeV/c, 1.2 MeV/c, 6.4 MeV/c, and 10.6 MeV/c respectively. The same values for the experimental distributions in the Q_t interval 0 – 1 MeV/c are significantly larger. In the DIRAC experiment, the main contribution to the width increase comes from the multiple scattering in the target. The multiple scattering in the detectors and the accuracy of the particle coordinate measurements are less important.

Table II shows the fitting procedure χ^2/ndf values for three data samples and five Q_t intervals

TABLE II.

ΔQ_t (MeV/c)	0 – 1.0	1.0 – 2.0	2.0 – 3.0	3.0 – 4.0	4.0 – 5.0
χ^2/ndf values					
Data 1	1.35	1.09	1.12	1.14	1.41
Data 2	1.45	0.90	1.29	0.90	1.19
Data 3	1.20	1.46	1.09	1.46	0.91

The χ^2/ndf values for four Q_t intervals from 0–0.25 MeV/c to 0.75–1 MeV/c are presented in Table III. At the given $ndf = 78$, the χ^2/ndf probability distribution is

close to the normal one with a mean of 1 and a standard deviation of 0.16. One may see from Tables II and III that the simulated Q_L distributions fit the experimental ones quite well despite their strong widening with increasing Q_t .

TABLE III.

ΔQ_t (MeV/c)	0 – 0.25	0.25 – 0.5	0.5 – 0.75	0.75 – 1.0
χ^2/ndf values				
Data 1	1.12	1.17	1.12	0.94
Data 2	1.30	1.10	1.06	1.10
Data 3	1.78	1.25	1.00	1.29

In each Q_t interval that has a large χ^2/ndf value for one data sample there are always two $\chi^2 = ndf$ values for the other data samples less than 1.32 and only one value 1.35. A slight excess over unity of the averages of the values in Tables II and III may be due to uncertainties in the detector resolution and efficiency, as well as in the correction factor $D(Q)$ in Eq. (4).

TABLE IV.

ΔQ_t (MeV/c)	0 – 1.0	1.0 – 2.0	2.0 – 3.0	3.0 – 4.0	4.0 – 5.0
$NC_{exp}(\Delta Q_t)$	75200	137900	215900	298000	368600
relative error	3.6%	2.2%	1.9%	1.7%	1.8%
$NC_{calc}(\Delta Q_t)$	75720	140030	217330	294760	367190

Using fitted fractions of *Coulomb pairs*, one may calculate their numbers $NC_{exp}(\Delta Q_t)$ - the experimental number of *Coulomb pairs* and the corresponding relative errors in the intervals ΔQ_t . Tables IV and V show $NC_{exp}(\Delta Q_t)$ values for the Data 3 sample ($NC_{calc}(\Delta Q_t)$ will be defined in section VI). It is seen that the relative precision of the number of *Coulomb pairs* decreases with decreasing Q_t because the background level becomes higher and the number of *Coulomb pairs* becomes smaller. The relative errors in the Data 2 sample are the same as in the Data 3 sample.

TABLE V.

ΔQ_t (MeV/c)	0 – 0.25	0.25 – 0.5	0.5 – 0.75	0.75 – 1.0
$NC_{exp}(\Delta Q_t)$	9460	21760	21130	25750
relative-error	10.5%	6.3%	6.2%	5%
$NC_{calc}(\Delta Q_t)$	7890	19480	23190	25160

The relative errors in the number of *Coulomb pairs* depend on the description of the experimental conditions, statistical errors and simulated distribution precision. In section IIB, reconstruction of the experimental Λ and $\bar{\Lambda}$ masses and widths and their comparison with the same simulated parameters were described. It was shown that the average correction to the simulated event widths is at the level of about 0.2%. It means that the setup geometry, momentum resolution and single-particle detection efficiency were defined well and the relative errors of the number of *Coulomb pairs* give the minimum accuracy of the theoretical approach. A conclusion that can be drawn

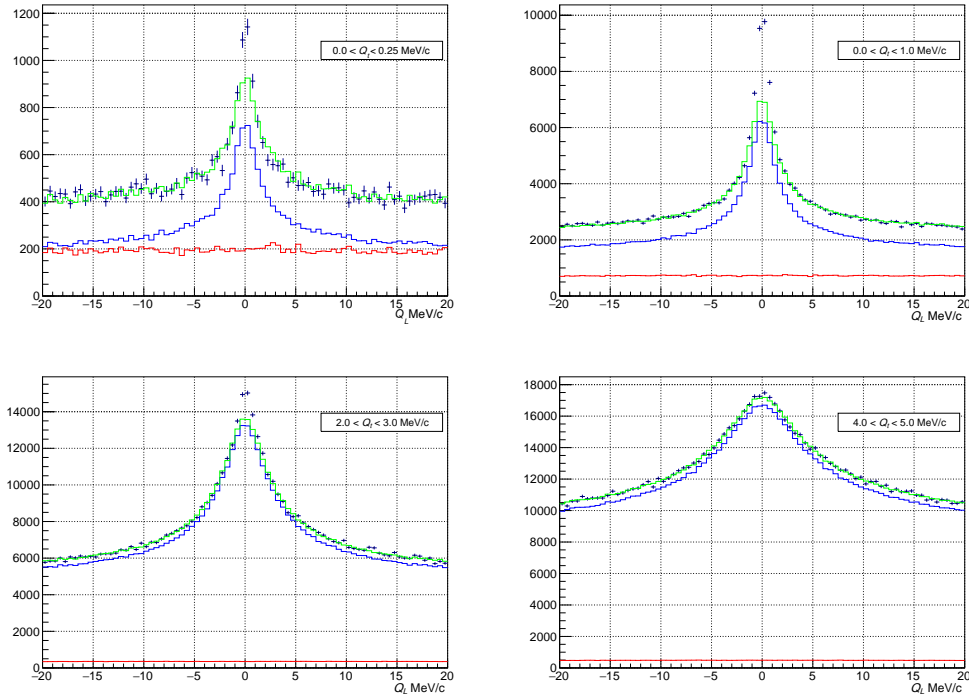


FIG. 3. The experimental Q_L distributions (black points with errors) of the *Coulomb*, *non-Coulomb* and *atomic* $\pi^+\pi^-$ pairs (sum of three data samples) for the Q_t intervals $0.0-0.25$ MeV/ c , $0.0-1.0$ MeV/ c , $2.0-3.0$ MeV/ c and $4.0-5.0$ MeV/ c . The green histogram is the corresponding combination of the *Coulomb* and *non-Coulomb* pairs simulated according to Eq. 4. The fraction of the *Coulomb* pairs and the normalization parameter were obtained by fitting in the total Q_L interval except for the region -2 MeV/ $c < Q_L < 2$ MeV/ c populated by the *atomic* pairs. One may see that the histograms well reproduce the increasing widths of the Coulomb peaks with increasing Q_t . The fitting histograms that describe the *Coulomb* (blue) and *non-Coulomb* (red) experimental pairs are presented as separate histograms. The excess pairs above the fitting histogram in the interval -2 MeV/ $c < Q_L < 2$ MeV/ c is due to the *atomic* pairs.

from the Data 2 and Data 3 analyses is that the theoretical approach using formula (4) allows one to describe the experimental distributions in Q_L and to obtain the number of *Coulomb* pairs with the precision better than 2% in Q_t intervals 2–3, 3–4 and 4–5 MeV/ c .

It allows one to use Coulomb pairs to study and correct the quality of the simulation events. The standard procedure to check and correct the simulation event quality is to compare the experimental and simulated particle mass distributions. The Coulomb pair analysis provides an additional possibility of checking the simulation accuracy. It has a special property which will be described in the next section.

VI. ANALYSIS OF EXPERIMENTAL Q_t DISTRIBUTIONS OF COULOMB PAIRS

In section V it was shown that the simulated distributions based on relation (4) described well Q_L distributions of *Coulomb* pairs for nine fixed Q_t intervals. In this section it will be shown [20] that formula (4) also describes the Q_t distribution of the experimental *Coulomb* pairs with Q_L belonging to the interval -20 MeV/ $c <$

$Q_L < 20$ MeV/ c . If Q_t decreases, the number of pairs with a small distance D between the tracks increases in the corresponding Q_t intervals. For these pairs, the detection efficiency ϵ has a strong dependence on D (see section IV), and errors in ϵ give rise to distortion of the number of simulated events and their greater difference from the number of experimental pairs. The analysis will also allow checking the accuracy of the ϵ dependence on D used in the DIRAC simulation procedure.

The fitting procedure described in section V was applied to the experimental Q_L distribution of the pairs (fitting interval -20 MeV/ $c < Q_L < 20$ MeV/ c , excluding the region -2 MeV/ $c < Q_L < 2$ MeV/ c) with the total Q_t interval $0-5$ MeV/ c to obtain $|M_{\text{prod}}|^2$ for the simulated events and to evaluate the expected numbers of *Coulomb* pair in different Q_t intervals. The results of the analysis are presented in Table VI.

It is seen in Table VI that the simulated distributions describe well all the experimental data in the Q_t interval $0-5$ MeV/ c . The fractions f of the *Coulomb* pairs in the three samples are in good agreement.

The average fraction of *Coulomb* pairs is $f = 94.4 \pm 0.5\%$, giving the average fraction of *non-Coulomb* pairs $1 - f = 5.6 \pm 0.5\%$. The analysis of the time spectra of

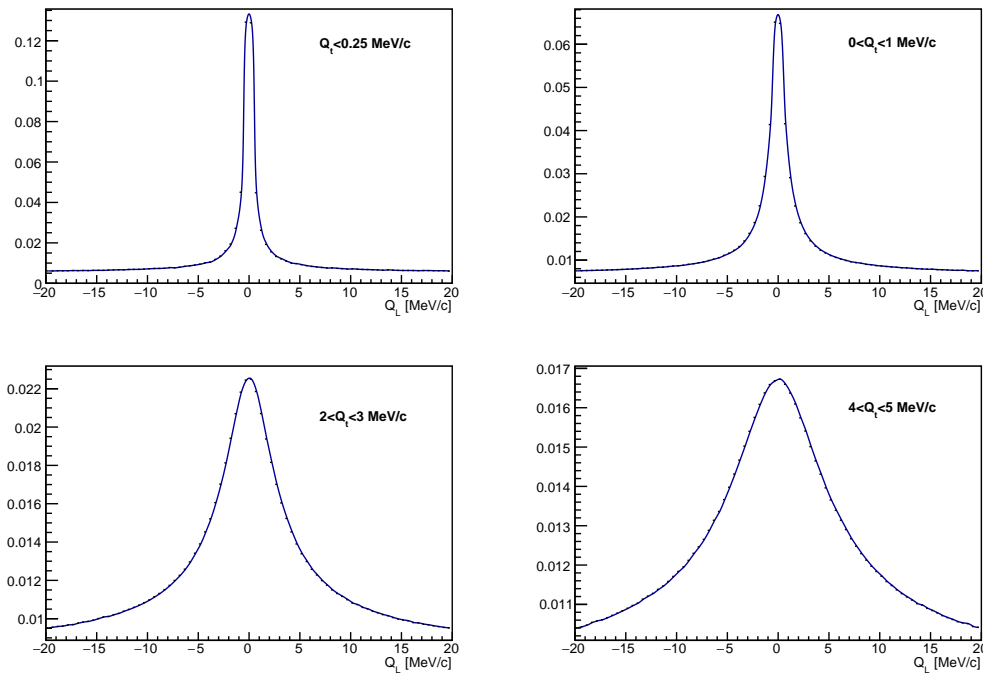


FIG. 4. The simulated Q_L distributions of $\pi^+\pi^-$ *Coulomb pairs* at the production point for Q_t intervals: $0 - 0.25$ MeV/c, $0 - 1$ MeV/c, $2 - 3$ MeV/c, $4 - 5$ MeV/c. All distributions are normalized to unity. It can be seen that the distribution width significantly increases with Q_t .

TABLE VI.

	Data 1	Data 2	Data 3
Number of <i>Coulomb pairs</i>	710300	1108400	1095000
χ^2/ndf	1.4	1.01	1.4
Number of non- <i>Coulomb pairs</i>	35010	72340	65260
Ratio $f = \text{Coulomb pairs}/\text{total pairs}$	$(95.3 \pm 1.1)\%$	$(93.9 \pm 0.9)\%$	$(94.4 \pm 0.9)\%$
Ratio $(1 - f) = \text{non-Coulomb}/\text{total pairs}$	$(4.7 \pm 1.1)\%$	$(6.1 \pm 0.9)\%$	$(5.6 \pm 0.9)\%$

prompt and *accidental pairs* gives for the relative contributions of *accidental pairs* to the interval of prompt pairs ± 0.5 ns, the values $(6.0 \pm 0.3)\%$ (Data 2) and $(6.2 \pm 0.6)\%$ (Data 3). These numbers show that *accidental pairs* make the main contribution to the *non-Coulomb pairs*, leaving only a percent level window for the contribution of long-lived sources. Since the effect of η' is taken into account in the factor $D(Q)$, this contribution is dominated by η -mesons, and their contribution is estimated to be less than a few percent [14].

The simulated distributions were obtained with the formula (4). To further check the precision of equation (4), the simulated Q_L distribution of the *Coulomb* and *non-Coulomb pairs* (in each data sample) was divided by the same experimental distribution.

The ratios for the three data samples as functions of Q_L are averaged and presented in Fig. 5, where for all the Q_L values in the fitting intervals (excluding region \pm

2 MeV/c) the ratios are about unity. The left and right sides of the ratios were fitted independently by a constant with a good χ^2 . The average ratio values for the negative and positive Q_L are 1.0000 ± 0.0021 and 1.0009 ± 0.0021 respectively [20]. One may conclude that formula (4) describes the Q_L distribution of the experimental events with a precision better than 0.5% for Q_t in the interval $0 - 5$ MeV/c.

The $|M_{\text{prod}}|^2$ evaluation allows calculating $NC_{\text{calc}}(\Delta Q_t)$ the expected number of the simulated *Coulomb pairs* in each of the ΔQ_t intervals analyzed in section V. The obtained $NC_{\text{calc}}(\Delta Q_t)$ were compared with the $NC_{\text{exp}}(\Delta Q_t)$ evaluated in section V by the fitting procedure in the same ΔQ_t intervals.

The results of the Data 3 analysis for nine ΔQ_t intervals are presented in Fig.6 and in Tables IV and V. It is seen that the differences between these numbers in all nine Q_t intervals are less than two standard deviations. The same good agreement is for the Data 1 and Data 2 samples.

In section V it was shown that the fitting procedure using formula (4) described the experimental distributions in Q_L with a precision better than 2% in the Q_t intervals $2-3$, $3-4$, and $4-5$ MeV/c. The agreement between $NC_{\text{calc}}(\Delta Q_t)$ and $NC_{\text{exp}}(\Delta Q_t)$ demonstrates that formula (4) describes the experimental data in the same Q_t intervals with a precision better than 2% also.

Fig.6 shows that the main contribution to $|M_{\text{prod}}|^2$ comes from the pairs with large Q_t . The distance D

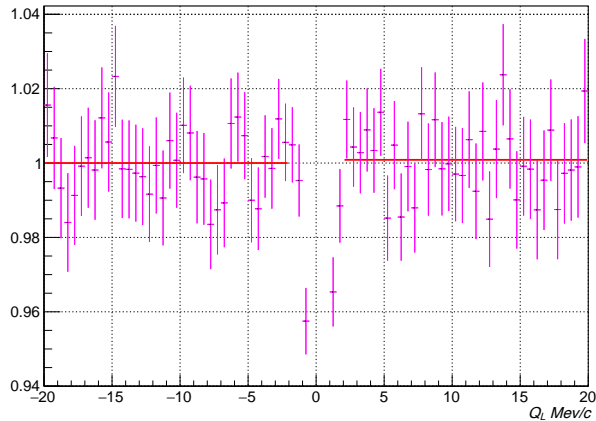


FIG. 5. The simulated Q_L distribution of the *Coulomb* and *non-Coulomb* pairs in each data sample was divided by the same experimental spectrum. The ratios for the three data samples as a function of Q_L were averaged and presented in this Figure. In the intervals of the positive and negative Q_L (excluding region $\pm 2\text{MeV}/c$), the points were fitted independently by a constant. It is seen that in the left and right intervals, the average ratios are unity, demonstrating that formula (4) describes the Q_L distribution well.

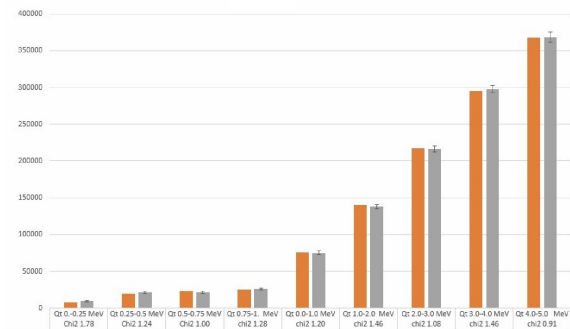


FIG. 6. The experimental numbers of *Coulomb* pairs $NC_{\text{exp}}(\Delta Q_t)$ for different Q_t intervals (gray). The calculated numbers of *Coulomb* pairs $NC_{\text{calc}}(\Delta Q_t)$ for the same Q_t intervals (brown).

of these pairs is large and the pair detection efficiency is well defined. The agreement between $NC_{\text{exp}}(\Delta Q_t)$ and $NC_{\text{calc}}(\Delta Q_t)$ for pairs with Q_t less than $0.5\text{ MeV}/c$ shows that the ϵ dependence on D at a small distance between tracks was taken into account correctly.

VII. THE VALUES OF THE ANGLES BETWEEN TWO TRACKS IN THE LABORATORY SYSTEM

The Q_t values in the c.m.s. and the l.s. are the same. Therefore, the pairs with minimal Q_t , have the minimum opening angles θ and distance D in the l.s. The total momenta of the experimental pairs are found mainly in the interval $2.4\text{--}8\text{ GeV}/c$ with an average of about $4\text{ GeV}/c$.

In interval (4) the average Q_t is $4.5\text{ MeV}/c$. The angle between two particles in the l.s. at this Q_t and the average total pair momentum is 2 mrad . The average Q_t in interval (1) is around $0.12\text{ MeV}/c$, and the opening angle for the average total pair momentum is 0.06 mrad . The contribution of the pairs with a smaller Q_t and a larger total momentum allows checking the detection efficiency for the pairs with the opening angles down to about 0.02 mrad . The distribution with large Q_t allows checking and correcting the simulation procedure for the pairs with large opening angles in the l.s. The detection efficiency for these pairs is the product of the well-known single-particle detection efficiencies. After the tuning of the simulation procedure and the evaluation of the $|M_{\text{prod}}|^2$ value using these pair distributions, the expected numbers of the simulated *Coulomb* pairs in the intervals with small Q_t can be calculated with the theoretical accuracy better than 2% . The comparison of the numbers of the simulated pairs NC_{calc} and the numbers of the experimental pairs NC_{exp} allows checking and correcting the detection efficiency for the pairs with a small distance D [20]. This possibility is the particular property of the method using *Coulomb* pairs.

VIII. CONCLUSION

In this work, the *Coulomb* effects in the $\pi^+\pi^-$ pairs were studied and their application to the data processing is justified. The $\pi^+\pi^-$ pairs were produced in p-Ni interactions with the proton momentum of $24\text{ GeV}/c$. The experimental data samples Data 1, Data 2 and Data 3 were obtained in three different runs. The *Coulomb* effects (*Coulomb* correlations) were studied using the experimental pair distributions in Q , the relative momentum in the pair c.m.s., and its longitudinal (Q_L) and transverse (Q_t) projections on the pair direction in the l.s. The major part of the $\pi^+\pi^-$ pairs was produced in decays of ρ, ω, Δ and other short-lived resonances (*Coulomb* pairs). In these pairs at small Q , the significant *Coulomb* interaction in the final state arises and increases the pair yield with decreasing Q . The minor part of the pairs contains one or both pions resulting from long-lived sources, such as η, η' or from different events (*non-Coulomb* pairs). In this case, the distance between particles would be much larger than the Bohr radius of the $\pi^+\pi^-$ atom, and the pion interaction in the final state is practically or completely absent.

The experimental $\pi^+\pi^-$ pair distributions were analyzed in the intervals $0 < Q_t < 5\text{ MeV}/c$ and $-20\text{ MeV}/c < Q_L < 20\text{ MeV}/c$ using a combination of the corresponding simulated *Coulomb* and *non-Coulomb* pair distributions. The simulated spectra of the *Coulomb* $\pi^+\pi^-$ pairs in the c.m.s. were obtained according to (4) with taking into account the $\pi\pi$ *Coulomb* and strong interaction in the final state and the nonpoint-like pair production.

The *non-Coulomb* pairs were simulated according to Eq.(4) without correlation, with $A_C(Q) = D(Q) = 1$.

All experimental events were divided into nine Q_t in-

tervals: 0–0.25, 0.25–0.5, 0.5–0.75, 0.75–1, 0–1, 1–2, 2–3, 3–4 and 4–5 MeV/c. In each interval, Q_L spectra were obtained, which showed peaks around $Q_L = 0$ caused by the Coulomb final state interaction (Fig. 3).

Each distribution was fitted (section V) by a combination of the simulated *Coulomb* and *non-Coulomb pairs* with two free parameters: the fraction of *Coulomb pairs* and the normalization constant. The fitting interval did not include the region $-2 \text{ MeV}/c < Q_L < 2 \text{ MeV}/c$ which contains atomic pairs that arose from the breakup of $\pi^+\pi^-$ atoms in the target (Fig. 1) and had a different shape of the Q_L and Q_t spectra.

Nine experimental distributions in all three data samples were described well. The full width at half maximum increases with Q_t and is 3.4 MeV/c ($0 < Q_t < 0.25 \text{ MeV}/c$), 4 MeV/c ($0 < Q_t < 1 \text{ MeV}/c$), 6.5 MeV/c ($2 < Q_t < 3 \text{ MeV}/c$) and 11 MeV/c ($4 < Q_t < 5 \text{ MeV}/c$). It appears that Eq. (4) describes the numbers of *Coulomb pairs* in Q_t intervals 2–3, 3–4 and 4–5 MeV/c with a precision better than 2%.

A dedicated analysis of the precision of Eq.(4) was done in the total Q_t interval 0–5 MeV/c using the fitting procedure described in section V. The fitted combination of the simulated Q_L distributions in each data sample was divided by the corresponding experimental spectrum. The averaged ratios for the three data samples were fitted by a constant, separately for positive and negative Q_L , excluding the region $Q_L < 2 \text{ MeV}/c$ (Fig. 5). The corresponding fitted ratios, 1.0000 ± 0.0021 and 1.0009 ± 0.0021 , and good quality of the fits demonstrate that the simulation procedure based on Eq. (4) describes the experimental Q_L distributions with the precision better than 0.5%.

The evaluated $|M_{\text{prod}}|^2$ in the Q_t interval 0–5 MeV/c allow the calculation of $NC_{\text{calc}}(\Delta Q_t)$, the expected number of the simulated *Coulomb pairs* in each of the nine ΔQ_t intervals. The obtained $NC_{\text{calc}}(\Delta Q_t)$ values were compared with $NC_{\text{exp}}(\Delta Q_t)$, the experimental numbers evaluated by the fitting procedure in the same ΔQ_t intervals (Fig. 6).

It is shown that in the three data samples and in all

nine Q_t intervals there is a good agreement between $NC_{\text{exp}}(\Delta Q_t)$ and the number of the simulated events $NC_{\text{calc}}(\Delta Q_t)$.

It demonstrates, together with the good χ^2 , that formula (4) describes the experimental Q_t and Q_L distributions of *Coulomb pairs* with a precision of better than 2% and the dependence of the two-particle detection efficiency ϵ on the distance D between the particles is taken into account correctly.

The pairs with the minimal Q_t have the minimum opening angles θ and the minimum distance D in the laboratory system. The total momenta of the experimental pairs are mainly in the interval 2.4 GeV/c – 8 GeV/c with an average value of about 4 GeV/c.

At $Q_t = 4.5 \text{ MeV}/c$ (interval 4.0–5.0 MeV/c) and the total momentum of 4.0 GeV/c, the angle θ is 2 mrad. At $Q_t = 0.12 \text{ MeV}/c$ (interval 0–0.25 MeV/c) the corresponding opening angle is 0.06 mrad. In this Q_t interval, there is a significant number of the simulated events with smaller Q_t and larger total momenta in the l.s. These pairs allow checking the detection efficiency for the pairs with the opening angles down to 0.02 mrad.

Finally, we have shown that the selection of $\pi^+\pi^-$ *Coulomb pairs* in different Q_t intervals less than 5 MeV/c allows one to form Q_L distributions of pairs with peaks around $Q_L = 0$ and with different widths. These distributions can be described with a theoretical precision better than 2% in the Q_t intervals 2–3, 3–4 and 4–5 MeV/c. In the same Q_t intervals, the number of *Coulomb pairs* can be calculated with the 2% accuracy. It is shown that for Q_t in the interval 0–5 MeV/c formula (4) describes the Q_L distribution of the experimental events with a precision better than 0.5%. The ordinary way to investigate the quality of the simulated events is based on comparing the reconstructed and simulated particle mass distributions. The properties of the Coulomb pairs allow one to use these pairs as a new physical tool to check and correct the simulated event quality. The particular property of the *Coulomb pairs* is the possibility of checking and correcting the detection efficiency for the pairs with small opening angles.

-
- [1] L. Afanasyev et al., Phys. Lett. B 255(1991)146.
[2] L. Nemenov, Yad. Fiz. 41 (1985) 980; Sov. J. Nucl. Phys. 41 (1985) 629.
[3] G. Gamov, Z. Phys. 51 (1928) 204.
[4] A. Sommerfeld, Atombau und Spektrallinien, F. Vieweg & Sohn (1931).
[5] A. D. Sakharov, Zh. Exp. Theor. Fiz. 18 (1948) 631,
[6] A. D. Sakharov, Sov. Phys. Usp. 34 (1991) 375.
[7] B. Andersson et al. Phys. Rep. 97(1983) 31-145.
[8] L. R. Wiencke, M. D. Church, E. E. Gottschalk, et al., Phys. Rev. D 46, 3708 (1992)
[9] L. Afanasyev et al., Phys. Lett. B 308 (1993) 200.
[10] B. Adeva et al., Phys. Lett. B 619 (2005) 50.
[11] B. Andersson et al., Nucl. Phys. B281(1987)289.
[12] B. Adeva et al., Phys. Lett. B 704 (2011) 24.
[13] R. Lednicky, J. Phys. G: Nucl. Part. Phys. 35 (2008) 125109.
[14] P.V.Chliapnikov, V.M.Ronjin, J.Phys.G: Nucl. Part. Phys. 36 (2009) 105004.
[15] M.V.Zhabitsky, DIRAC notes 2007-01, 2007-11; <http://cdsweb.cern.ch/record/1369660>
[16] M.V.Zhabitsky, Phys. At. Nucl. 71 (2008) 1040
[17] B. Adeva et al., Nucl. Instr. Meth. A 839 (2016) 52
[18] B. Adeva et al., Phys. Rev. D96 (2017) 052002.
[19] A. Benelli and V. Yazkov, Report No. DN-2016-01; <http://cds.cern.ch/record/2137645>
[20] A. Benelli, L. Nemenov, M. Pentia, J. Smolik, DIRAC Note 2023-01; <http://cdsweb.cern.ch/record/xxxxxxx>
[21] O. Gorchakov and A. Kuptsov, DIRAC Note 2005-05; <http://cds.cern.ch/record/1369686>.

- [22] O. Gorchakov, DIRAC Note 2005-23; <http://cds.cern.ch/record/1369668>.
- [23] M. Pienta et al., Nucl. Instr. Meth. A 795 (2015) 200.
- [24] DIRAC Collaboration; <http://dirac.web.cern.ch/DIRAC/offlinedocs/Userguide.html>.
- [25] A. Benelli, J. Smolik V. Yazkov, DIRAC Note 2020-01; <http://cds.cern.ch/record/2772989>.
- [26] P. Doskarova and V. Yazkov; DIRAC Note 2013-05; <http://cds.cern.ch/record/1628541>.
- [27] A. B. Arbuzov, Nuovo Cim. A 107 (1994), 1263-1274
- [28] S.A. Bass et al., Prog. Part. Nucl. Phys. 41 (1998) 225